Bolton, M. D., Nakata, Y. & Cheng, Y. P. (2008). *Géotechnique* **58**, No. 6, 471–480 [**doi:** 10.1680/geot.2008.58.6.471]

Micro- and macro-mechanical behaviour of DEM crushable materials

M. D. BOLTON*, Y. NAKATA† and Y. P. CHENG‡

This paper provides a micro-mechanical commentary on the macroscopic behaviour observed in DEM simulations of the compression of individual crushable grains, and of triaxial tests on assemblies of both crushable and uncrushable grains. A fragmentation ratio is defined to describe the bond breakage processes, and the significance of other micro-mechanical parameters such as sliding contacts ratio, average coordination number, deviator fabric, and internal energies per unit volume is discussed. Three different modes of grain damage were observed: asperity breakage, internal shear cracking, and internal tensile cracking leading to fast fracture. Energy balances both for the compression of a single grain, and for triaxial tests on assemblies of grains, showed that the loss of elastic energy due to bond breakage was a negligible fraction of the significantly enhanced dissipation encountered with crushable materials. This extra dissipation was associated with frictional sliding triggered by the creation of new degrees of freedom among the breaking fragments. Different modes of grain breakage were found to be representative of different regions of soil states of stress defined with respect to the virgin compression line. The secondary role of elastic grain deformability, increasing coordination number but reducing dilatancy, has also been demonstrated.

KEYWORDS: constitutive relations; fabric/structure of soils; friction; numerical modelling; particle crushing/crushability; plasticity

La présente communication présente un commentaire micromécanique sur le comportement macroscopique observé dans des simulations de DEM sur la compression de grains déformables individuels, ainsi que des tests triaxiaux sur des ensembles de grains déformables et non déformables. On y définit un taux de fragmentation pour décrire les procédés de rupture des liaisons, et on discute de l'importance d'autres paramètres micromécaniques, par exemple le taux de contacts glissants, le nombre moyen de coordinats, la structure de déviateurs, et les énergies internes par volume unitaire. On a relevé trois modes divers d'endommagement de grains : rupture d'aspérités, fissuration de cisaillement interne, et fissuration sous traction interne entraînant une fracture rapide. Des bilans énergétiques à la fois pour la compression d'un grain unique et pour des tests triaxiaux sur des ensembles de grains ont permis de démontrer que la perte d'énergie élastique due à une rupture de liaison représente une fraction négligeable de la dissipation sensiblement accrue que l'on rencontre dans les matières déformables. Cette dissipation supplémentaire dépend du glissement par frottement déclenché par la création de nouveaux degrés de liberté entre les fragments de rupture. On a établi que différents modes de rupture du grain étaient représentatifs de différentes régions d'états des sols, définies en fonction de la ligne de compression vierge. On a également démontré le rôle secondaire de la déformabilité élastique du grain, qui augmente la coordinance tout en réduisant la dilatance.

INTRODUCTION

Constitutive models define the relationship between external excitations and the response of a material. Although the material response of soils is conventionally described in terms of the macro-scale measurements of stress and strain inferred at the boundaries of elements, better constitutive models also include micro-scale parameters, representing changes in internal structure so that phenomena such as anisotropy, yielding, hardening and softening can be captured by physically meaningful parameters. Internal structure is reflected by various measures of soil fabric, including the grain-size profile, the voids ratio, the spatial distribution of grains and voids, and the coordination number of grains. Although many researchers have studied how these basic factors act as internal variables, they have typically assumed an unchangeable grain-size profile under all loading cases.

In many geotechnical engineering applications, such as penetrometer testing, piledriving and end bearing resistance, and high earth or rockfill dams, soils may experience stresses high enough to break particles of even the strongest soil minerals (Randolph *et al.*, 1994; Yasufuku & Hyde, 1995; Leung *et al.*, 1996; Ohta *et al.*, 2001). There are also many weak-grained crushable soils, such as decomposed granites, carbonate sands or volcanic ashes, for which particle crushing can be important even under low stress conditions. For these reasons, the effect of particle crushing on the deformation response of soils should not be neglected. This is true because a change in grain size distribution due to crushing may create a more drastic change in internal structure than can be achieved by particle rearrangement alone.

The distinct element method (DEM) has been adopted recently by various researchers to simulate the behaviour of crushable soil. The pioneering work of Robertson (2000) explored the procedure of modelling crushable numerical grains created by bonding elementary balls and introducing probabilistic flaws. Research by McDowell & Harireche (2002a, 2002b) then suggested a procedure to create agglomerates of different sizes with crushing strengths that follow Weibull statistics. The characteristic yield stress of an assembly of agglomerates, which they defined as the point of maximum curvature on an e–$\log p$ plot, was shown to be proportional to the characteristic (37th percentile) compressive strength of a corresponding batch of single-agglomerate crushing tests. Cheng *et al.* (2003) modelled the statistical strength of silica sand grains having a Weibull modulus of 3 (Nakata *et al.*, 2001a) and discussed the macro-scale deformation characteristics of an assembly of DEM agglomerates during isotropic compression and conventional triaxial com-

Manuscript received 25 May 2005; revised manuscript accepted 28 February 2008.
Discussion on this paper closes on 2 February 2009, for further details see p. ii.
* Department of Engineering, University of Cambridge, UK.
† Graduate School of Science and Engineering, Yamaguchi University, Japan.
‡ Department of Civil, Environmental and Geomatic Engineering, University College London, UK.

pression. It indicated the potential of using DEM simulations to understand plastic behaviour of crushable soils seen in laboratory tests. Cheng *et al.* (2004) went on to show that a lightly overconsolidated assembly of DEM agglomerates had an elliptical yield surface as described by Modified Cam-Clay, but with a non-associated plastic potential surface. Heavily overconsolidated DEM agglomerates were shown to follow a dilatancy rule similar to that described by Rowe (1971), and a dependence of the peak angle of internal friction on effective stress level due to the influence of grain crushing as described by Bolton (1986).

Simulating crushable soils using DEM has therefore become a powerful tool that provides valuable insights into the micro-mechanical origins of soil plasticity. It is therefore timely to engage in a more in-depth micro-mechanical discussion in terms of agglomerate fragmentation and micro-parameters such as coordination number, fabric tensor, and the energy dissipated due to the breakage of agglomerates. This paper provides both micro- and macro-mechanical discussions for a newly computed assembly of DEM agglomerates, the assembling process of which differed slightly from that of Cheng *et al.* (2003, 2004).

NUMERICAL GRAIN MODELLING AND MECHANICAL BEHAVIOUR

Modelling crushable materials

The PFC^{3D} program, following Cundall & Strack (1979), was used here to simulate the behaviour of a system of crushable agglomerates with DEM parameters, as used by Cheng *et al.* (2003) and Cheng (2004), and summarised in Table 1. Fig. 1 shows the normal and shear force diagram for a contact. When a simple contact bond exists, the magnitudes of the tensile and shear contact forces are limited by the normal and shear bond strengths b_n and b_s respectively. Here, the values are taken as equal, so that $b = 4$ N, as shown in Fig. 1. The slip model is active when the contact bond is broken or does not exist, and is represented by the slip-line in Fig. 1. The linear contact stiffness model is defined by normal and shear stiffnesses k_n and k_s (each taken here as $k = 4 \times 10^6$ N/m) at each ball: this means that two elastic springs exist at each contact, regardless of the presence of a bond. The elastic springs store an amount of energy proportional to the square of the contact force. Fig. 1 shows the contours of the stored elastic energy.

Table 1. DEM parameters used (Cheng *et al.*, 2003)

Diameter of agglomerate: mm	1·0
Diameter of sphere: mm	0·2
Density of sphere: kg/m^3	2650
Maximum number of spheres in an agglomerate	57
Maximum number of bonds in an agglomerate	228
Normal and shear bond strength: N	4
Normal and shear stiffness of each sphere: N/m	4×10^6
Frictional coefficient of sphere	0·5
Percentage of spheres removed at random: %	20

If the magnitude of the tensile contact force equals or exceeds the normal contact bond strength, or the magnitude of the shear contact force equals or exceeds the shear contact bond strength, then the bond breaks and disappears. In reality, the elastic strain energy that is released when brittle materials fracture is converted into surface energy and acoustic energy. In the DEM simulation, the sudden breakage of a bond also implies a sudden loss of stored elastic energy. For a broken tensile bond, for example, the total loss of elastic strain energy is $\delta B = b^2/k$ considering both contact springs. This is illustrated in Fig. 1, when the contact forces in bond no. 116 drop axiomatically to zero after breakage and 'release' approximately 5×10^{-6} N m of stored elastic energy. On the other hand, bond no. 127, which was broken in shear, lost only a proportion of its initial strain energy as its contact stress fell to the Coulomb friction slip-line. The sudden imbalance of tangential forces at such a contact will lead to slippage, frictional dissipation, and an increase in kinetic energy as calculated from the particle velocities at the next time step.

In reality, the kinetic energy of fast-moving grains is quickly converted into heat through friction. In the DEM simulation a similar mechanism can apply, through damping forces introduced as a proportion (0·7) of out-of-balance forces. Kinetic energy was thereby maintained at negligible levels. As a result, any kinetic energy released as a consequence of DEM bonds breaking contributes to the energy loss due to the rearrangement of balls. Further study of the sensitivity to the damping factor can be found in Cheng (2004).

It is beneficial to consider the changes in four components of work and energy during simulated tests on DEM agglomerates: δW, work input at the test boundaries; δS, change in energy stored as elastic strain energy at points of contact; δB, energy lost due to material damage, here in the form of bond breakage; and δF, energy lost in friction and damping due to the rearrangement of balls.

Applying the first law of thermodynamics to these components we obtain

$$\delta W = \delta S + \delta B + \delta F \tag{1}$$

noting that the numerical simulations admit no other component of internal energy. For completeness it should be noted that whereas δW and δS might take either positive or negative values, δB and δF must be positive for any loading or unloading step, by definition. For this reason, the last two terms can be combined as dissipation, $\delta D = \delta B + \delta F$, so that

$$\delta W = \delta S + \delta D \tag{2}$$

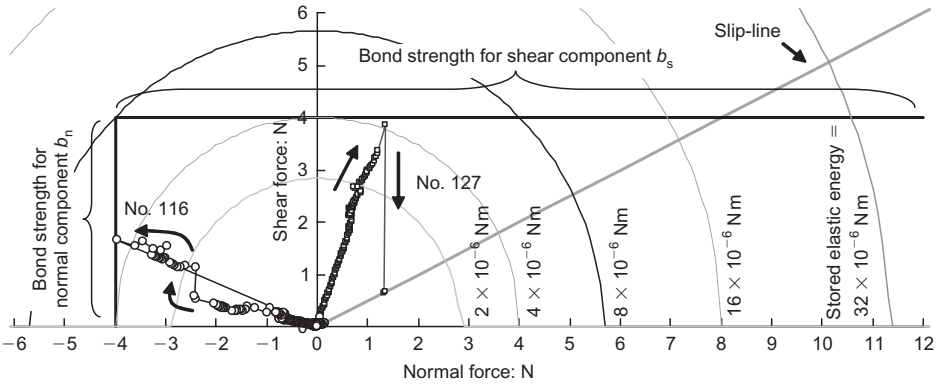

Fig. 1. Bond strength, slip-line and force paths on normal and shear force diagram

This is superficially analogous to conventional soil plasticity theory, such as Cam Clay following Roscoe *et al.* (1963), where a work increment is written

$$\delta W = \delta U + \delta P \tag{3}$$

where δU is recoverable (elastic) work and δP is irrecoverable (plastic) work. The macroscopic terms δW, δU and δP are given by the boundary measurements, whereas the summed microscopic terms δS and δD are obtainable only by DEM simulations. The 'stored plastic work' of Collins (2005) can be understood as a fraction of the elastic strain energy δS currently stored at contacts, but which will be unavoidably dissipated through particle rearrangements before it can be returned as work at the boundaries.

Crushing a numerical agglomerate

Figure 2 shows the stress–compression relationship of a nominal 1 mm diameter agglomerate in the same batch reported by Cheng *et al.* (2003). This agglomerate had 45 balls and 148 bonds, equivalent to the average number of spheres and bonds in the batch (see Cheng *et al.*, 2003). The small increases and sudden decreases of stress at the beginning were due to rotations of the agglomerate (at B, C and D) to accommodate compression by the smooth walls, triggered in one case by the shearing of a superficial ball analogous to the breakage of an asperity on a real sand grain. After 0·08 mm of wall displacement the stress started to increase again with a steeper slope than before, up to 0·1 mm, marking the end of purely elastic deformation in that phase of the test. Each square icon in Fig. 2 then represents a contact bond broken by shear, whereas a circular icon represents a contact bond broken by tension. Unstable fracture began at 0·13 mm compression when the stress dropped as contact bonds continued to break. The figure shows that the predominant bond-breaking mode was in shear when stress was increasing in a stable manner, but in tension when stress was dropping in an unstable manner. The internal shearing and progressive cracking of the agglomerate might be described as damage by crushing. Finally, tensile fast fracture splits the agglomerate.

The various components of microscopic work are shown in Fig. 3(a), where the asterisk * denotes the work and energy per agglomerate under diametrical crushing. Fig. 3(b) shows the number of unbroken contact bonds that exist at each stage. All quantities are plotted against the relative displacement of the platens during the compression process.

Between 0·08 mm and 0·10 mm the rate of increase of stress (in Fig. 2) is at its largest when the well-located agglomerate responds elastically. The similarity in the rate of increase of boundary work W^* and the rate of storage of elastic energy S^* in the springs prior to significant bond breakage is typical for an elastic material. The small difference is due to initial kinetic energy as the agglomerate slips and rotates between the platens. Between 0·10 mm and 0·135 mm the number of intact bonds reduces from 145 to 117 at the point of maximum stress, at 0·135 mm compression in Fig. 3(b). The stress increases with gentler slope in Fig. 2 when bonds progressively break in shear. Fig. 3(a) shows that, at this stage, a small amount of elastic energy B^* is released, while the accumulated dissipation F^* arises mostly from frictional sliding at contacts where bonds have broken. Then the agglomerate experienced fast fracture during which the number of intact bonds decreased drastically from 117 to 77 within the displacement interval 0·1358 mm to 0·1398 mm.

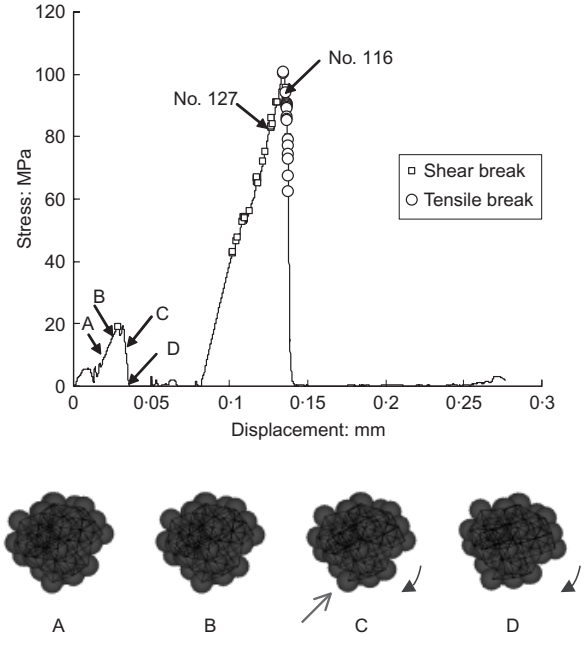

Fig. 2. Breaking mode of bonds, and stress–compression relationship

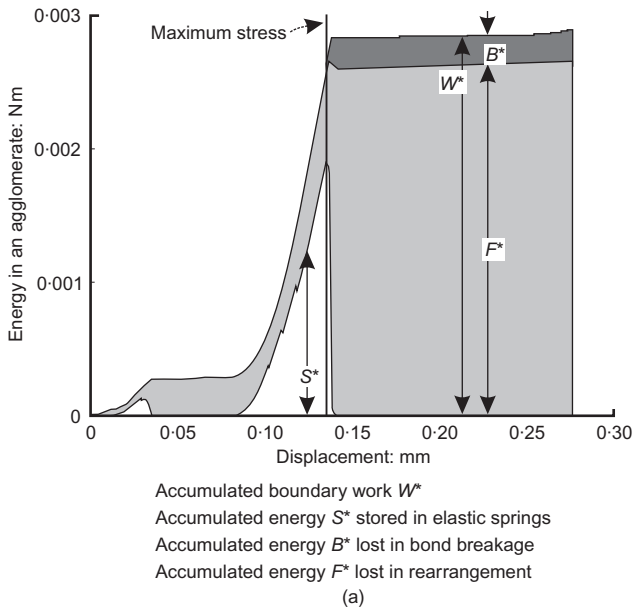

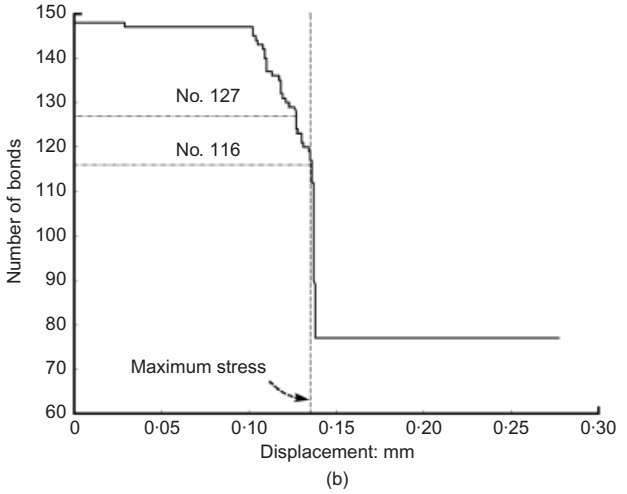

Fig. 3. Crushing process for a numerical agglomerate: (a) boundary work and energy components; (b) number of surviving bonds

Between 0·08 mm and 0·135 mm of compression, 0·0025 N m of boundary work W^* was input into the agglomerate. The elastic springs stored energy S^* of about 0·0018 N m, which contributed 75% of the total. Prior to fast fracture at this stage, the dissipated energy B^* released by material damage was only 3% of W^*. The energy balance therefore shows that 22% of W^* was dissipated through F^* either by friction during rearrangement of the broken balls or by damping. Damping dissipation would be small at this stage. After fast fracture, beyond displacement 0·1398 mm, W^* kept approximately constant. The elastic energy S^* dropped to zero, whereas the dissipation B^* rose to 10% of the boundary work W^*, and the dissipation F^* now accounts for 90% of the boundary work. During fast fracture the damping dissipation can be large, but the outcome is clear. The energy B^* released by simulated micro-cracking and fast fracture is an order of magnitude smaller than the energy F^* dissipated as the micro-cracks overcome friction and slide, as the fragments burst away and slow down. Damage B^* acts as a trigger, creating new degrees of freedom, and consequently is responsible for the much larger frictional dissipation F^* that follows.

Although this idealisation may have limitations, owing to the limited number of balls in an agglomerate, Cheng *et al.* (2004) have reported that the macroscopic behaviour of an assembly of these model grains was very similar to real crushable soil. The high proportion of frictional energy dissipated during quasi-static diametrical compression of grain-size agglomerates also agrees with the numerical simulations of dynamic impact fracture of nano-scale agglomerates (Thornton *et al.*, 1996), and with the analysis of experiments on silica sand (McDowell *et al.*, 2002).

MECHANICAL BEHAVIOUR OF AN ASSEMBLY OF AGGLOMERATES

Isotropic compression

Isotropic compression tests were simulated for a cubical element comprising 378 agglomerates, identical to that of Cheng *et al.* (2003). During the numerical sample preparation stage the six rigid walls were moved inwards at a slow speed of 0·01 m/s until the aggregate reached a voids ratio of 2·0. Cheng *et al.* (2003) and Cheng (2004) had used much higher platen speeds of up to 2 m/s to demonstrate small dynamic effects due to unbalanced forces, and had then made triaxial simulations with a platen speed of 1 m/s. The aim of imposing a much slower speed was to maintain a more homogeneous and isotropic internal structure. After this stage, the isotropic compression was carried out with 0·05 m/s wall speed, i.e. with 0·1 m/s approach speed of every pair of walls, on each axis.

Figure 4 shows the isotropic compression curve for three particulate media having different crushing properties. The data are shown with a natural scale for stress in Fig. 4(a), and a logarithmic scale in Fig. 4(b). The thick black line shows the compression results for the assembly of crushable agglomerates with 20% of the balls removed randomly from the regular array, as described earlier. These agglomerates were intended to capture some effects of the randomness of shape and internal flaws in real sand grains. The compression behaviour compares very well with that of real soils as reported by McDowell & Harireche (2002b) and Cheng *et al.* (2003). The thin black line that starts from the same voids ratio of 2·0 represents the compression curve of the same assembly of agglomerates with the same proportion of elementary balls removed, but with unbreakable contact bonds. The volumetric decrease is significantly smaller, as the micro-mechanism was restricted to elasticity at the contacts and rearrangement of the very irregular agglomerates. Comparing the two lines shows that crushability is essential for a realistic representation of plastic deformation with DEM.

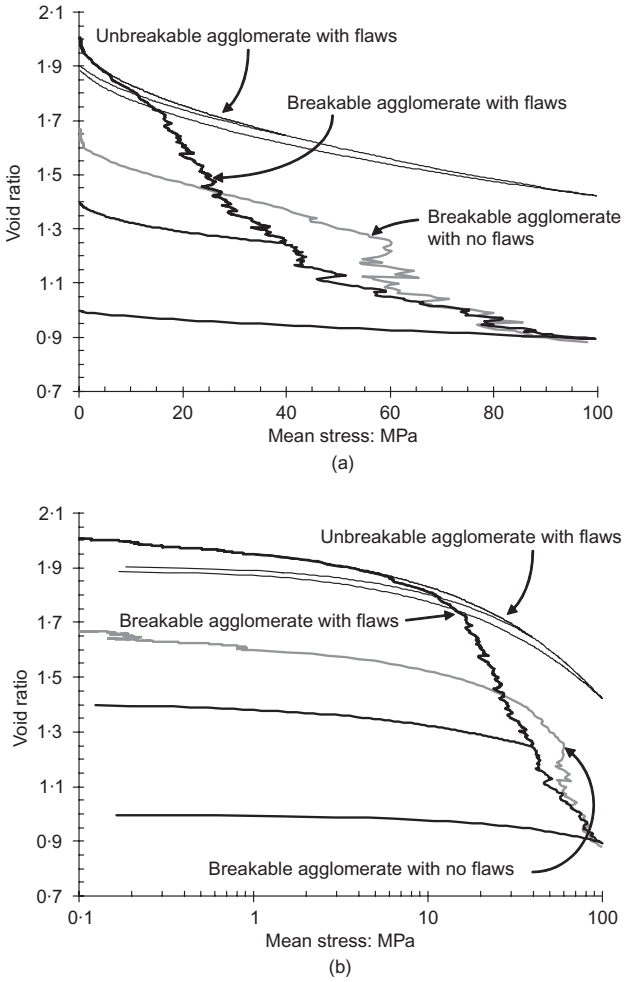

Fig. 4. Validity of randomness and crushability in modelling: (a) isotropic compression curve with natural scale of stress; (b) isotropic compression curve with logarithmic scale of stress

The evolution of fragmentation of the assembly, corresponding to the thick black line of Figs 4(a) and 4(b), is given in Fig. 5(a), which shows the degree of fragmentation of the agglomerates on an e–$\log p$ relationship. The fragmentation ratio at instances of fragmentation is represented by the size of the bubbles, and is defined as the number of balls in the smaller broken piece (the child agglomerate) divided by the number of balls in the original piece (the parent agglomerate) just before it broke:

$$\text{fragmentation ratio} = \frac{\text{number of balls in the smaller child agglomerate}}{\text{number of balls in the parent agglomerate}} \quad (4)$$

As the parent agglomerates get smaller, the numbers are constantly redefined. Fig. 4(a) shows that the e–p curve of the breakable agglomerates first deviated from that of the unbreakable agglomerates at 6 MPa. Successive stress increments then induced breakage with a small fragmentation ratio. In order to show the size of any broken parent agglomerate, the degree of fragmentation is drawn in Fig. 5(b), plotting the number of balls in the parent agglomerate against the logarithm of applied mean pressure. At 6 MPa, when the first grain crushed, the number of elementary balls existing in each parent agglomerate was relatively large, and well within the initial distribution of 34 to 54. This phase of asperity damage finishes at a stress of about 17 MPa, when

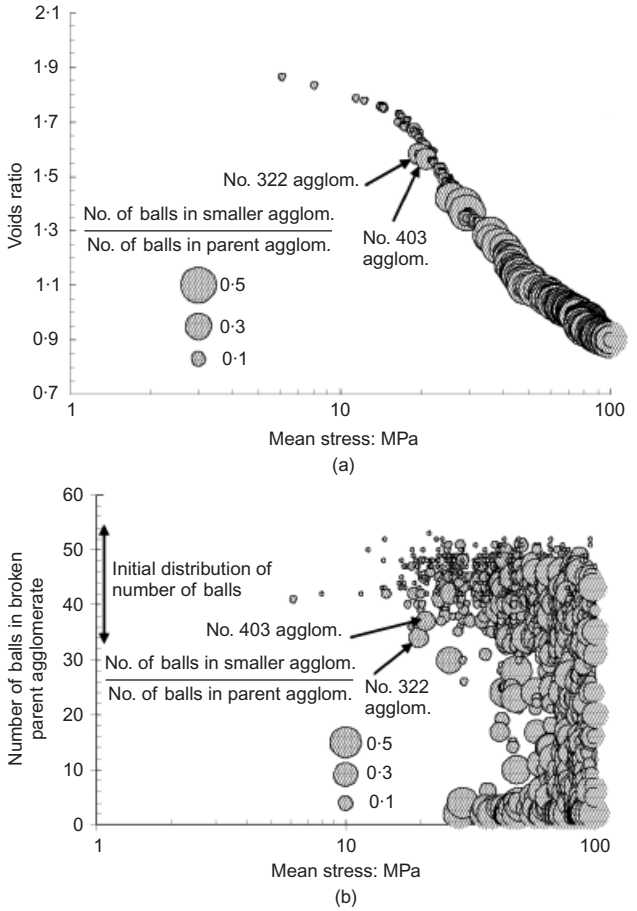

Fig. 5. Degree of fragmentation during isotropic compression: (a) voids ratio against logarithm of mean stress; (b) size of broken parent agglomerate against logarithm of mean stress

the rate of compression increases suddenly, as seen in Fig. 4(a). This also coincides with the first two incidents of grain splitting for agglomerates no. 322 and no. 403 with a fragmentation ratio of 0·2. Fig. 4(a) shows that this new regime of linear compression lasts from about 17 MPa to about 31 MPa, during which interval Fig. 5 clarifies that incidences of grain splitting became more frequent until about 40 MPa, when they were occurring for every size of agglomerate. Beyond 40 MPa all possible events of asperity damage and grain splitting can occur at every grain size, as Fig. 5(b) shows, while Fig. 4(a) shows progressive hardening. This last phase of compression plots as approximately linear on a logarithmic stress axis in Fig. 4(b), so it can be associated with 'normal compression' of the assembly of aggregates, with a slope λ of 0·4. This qualifies the hypothesis by McDowell & Bolton (1998) that 'normal compression' occurs when the stresses are high enough that every grain has a chance of splitting, and is consistent with the experiments of Nakata *et al.* (2001a).

The thick grey line of Fig. 4 represents an assembly of agglomerates without removal of any elementary balls from the regular array, although the bonds are crushable. The initial voids ratio of these more perfect agglomerates was much less than that of the flawed agglomerates. There was also an apparent 'de-structuring' effect during the clastic yielding process. The sudden drop in volume at a nearly constant mean stress of 60 MPa is due to the more uniform crushing strength (characteristic strength 203 MPa, Weibull modulus 9·4) of these more perfect agglomerates. A similar phenomenon was seen in the compression of glass beads that also have a relatively uniform distribution of crushing strength (Weibull modulus 5·9), as reported by Nakata *et al.* (2001b), compared with the imperfect agglomerates and the silica sand, each of which had a Weibull modulus of about 3. McDowell & Bolton (1998) had noted that granular materials with a high Weibull modulus should be expected to show catastrophic volumetric compression at the onset of grain breakage. A similar sudden drop in volume has also been observed for undisturbed clay, sedimentary soft rock and cemented soils (e.g. Leroueil & Vaughan, 1990), and attributed to ageing or cementation. The current work emphasises that catastrophic compression may best be attributed to a lack of statistical variation in local crushing strength. The importance of variability in the statistical distribution of the compressive strength of elements within the overall structure of a geomaterial deserves further attention.

Returning to the isotropic compression of randomised agglomerates, as presented in Figs 4 and 5, Fig. 6 shows the history of bond breakage for agglomerate No. 322 before it split into two large pieces at around 17 MPa as the 21st bond of the agglomerate was broken. As the number of the broken bonds inside the agglomerate increased, the tensile breaking mode began to dominate (from 17th to 21st broken bond) before the split. This confirms that the collective tensile breaking of bonds leads to splitting of agglomerates, just as it does in single agglomerate crushing. This common micro-mechanical feature justifies the comparison between the characteristic (37th percentile) crushing strength of individual grains and the yield stress of uniformly graded particulate media, as tested experimentally by Nakata *et al.* (2001b) and McDowell (2002), and the normalisation of the mean macroscopic stress by the 37% crushing strength for DEM crushable materials calculated by McDowell & Harireche (2002b) and Cheng *et al.* (2003).

After successive fragmentation generations, the size distribution of the agglomerates on the normal compression line is as shown in Fig. 7. The horizontal axis is the representative size, defined as the 1/3 power of the current solid volume of each individual agglomerate, and the vertical axis is the per-

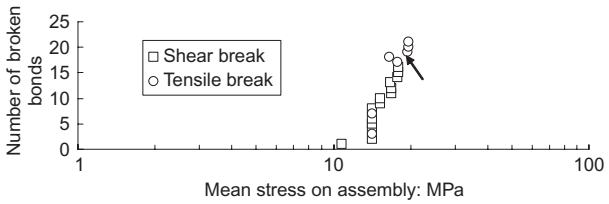

Fig. 6. Bond-breaking modes for agglomerate no. 322 during isotropic compression

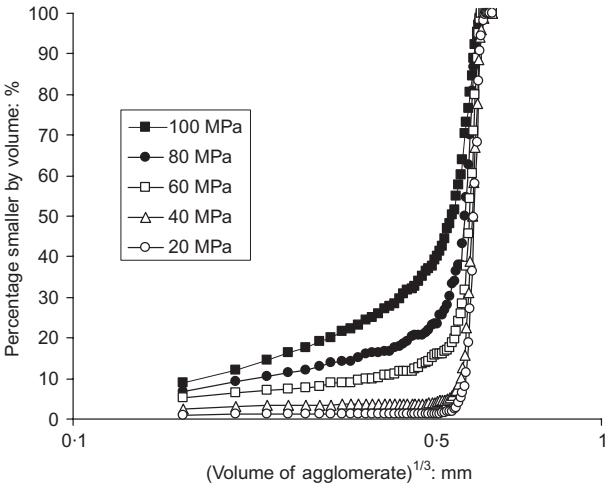

Fig. 7. Distribution of effective grain size, defined as (volume of agglomerate)$^{1/3}$

centage by volume of sizes smaller than the current size. The curves correspond conceptually to the particle size distribution curves in sieving analyses. Initially, the agglomerates were nearly uniform in size. As mean stress increased, the agglomerates became well distributed in size. This is similar to the evolution of real particle size distributions. The smallest size, however, was restricted by the size of the elementary sphere.

Triaxial compression

In order to understand more deeply the significance of the introduction of crushability into DEM simulations, constant mean stress triaxial compression shearing tests were simulated for both breakable and unbreakable agglomerate assemblies after they were normally compressed to various pressures along the thick and thin black lines respectively in Fig. 4. In order to keep the mean stress constant during shear, a servo-control algorithm was adopted. Fig. 8 shows the results for the breakable agglomerate assembly compressed by rigid walls giving: (a) the deviator stress–strain curves, and (b) the curves of volumetric strain against deviator strain. The volumetric behaviour with confining pressures of 1 and 5 MPa was dilative, with no obvious peak in the stress–strain relation. This is due to the lack of opportunity for the element to develop shear bands, first because the dimension ratio of the specimen to the agglomerate is too small, as also found in the experimental data of Hettler & Vardoulakis (1984), and second because the element was surrounded by rigid walls rather than by a simulated rubber membrane. As the confining pressure increased, the drained behaviour changed from dilation to show contractions of volume as large as 15% at confining pressures of 20 and 40 MPa. This is to be attributed to repacking of broken fragments. Corresponding results for the unbreakable agglomerate assembly are given in Fig. 9.

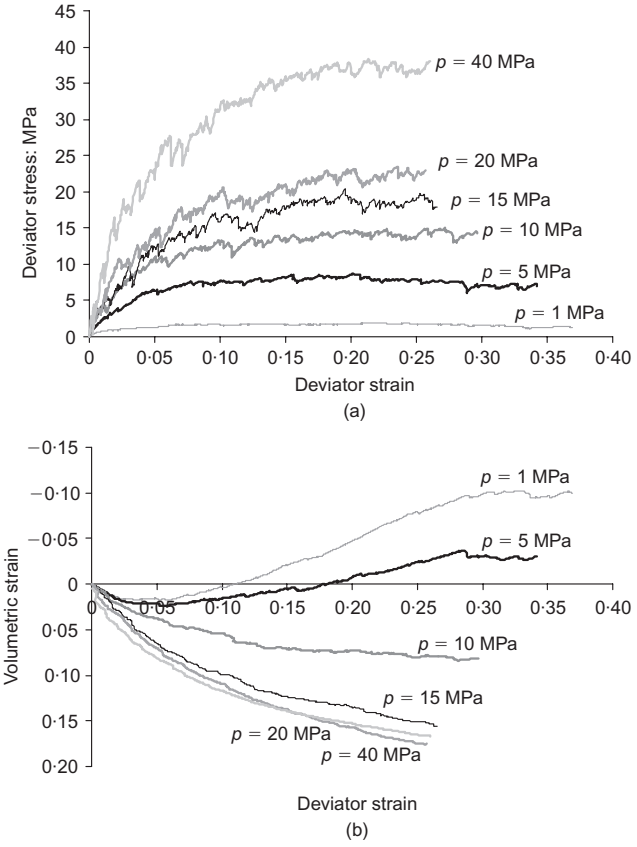

Fig. 8. Behaviour of breakable materials subjected to constant mean stress triaxial compression: (a) deviator stress and deviator strain for breakable agglomerates; (b) volumetric strain and deviator strain for breakable agglomerates

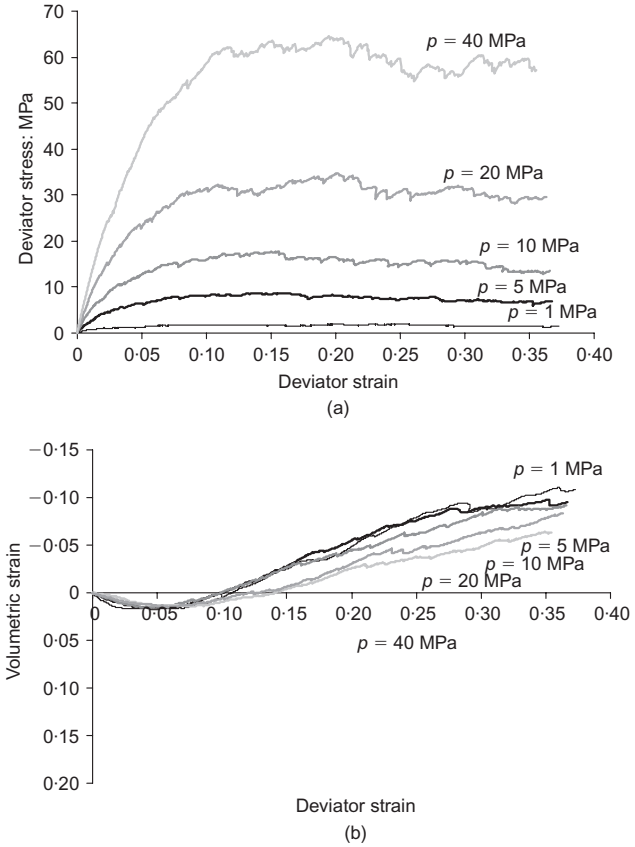

Fig. 9. Behaviour of unbreakable materials subjected to constant mean stress triaxial compression: (a) deviator stress and deviator strain for unbreakable agglomerates; (b) volumetric strain and deviator strain for unbreakable agglomerates

Shearing at all levels of initial confining pressure then produced volume dilation, reducing slightly as the confining pressure increased. This can only have resulted from elastic particle distortion mitigating the tendency for overriding during grain rearrangement. Again, post-peak softening was not very distinct in these assemblies retained within rigid walls.

Figure 10 shows the degree of fragmentation, defined in equation (4) and shown for isotropic compression in Fig. 5, during triaxial compression (a) at 5 MPa, (b) at 10 MPa, and (c) at 20 MPa. As the confining pressure increased, the frequency of fragmentation increased. In the test at 5 MPa, most fragmentation consisted of a few balls breaking off from their parent agglomerate, similar to surface scratching or the breakage of asperities on real grains. Particle splitting (i.e. a fragmentation ratio of about 0·5) occurred only once, at 17% deviator strain, for an agglomerate that consisted of only two balls. In the test at 10 MPa, although most damage was again superficial, a few large agglomerates also split. This happened beyond the critical pressure of about 8 MPa (Cheng *et al.*, 2005). The progress of fragmentation when shearing at 10 MPa (Fig. 10(b)) seems to be transitional towards that at 20 MPa, for which Fig. 10(c) shows agglomerates of all sizes splitting, as was the case in isotropic compression at 40 MPa. Although the micro-mechanics for isotropic and triaxial compression may be different in some respects, a common fragmentation process is observed, as also seen in sieving analyses.

MICRO-MECHANICAL PARAMETERS OF AN ASSEMBLY OF AGGLOMERATES

Although there have been reports of micro-mechanical investigations using DEM (e.g. Rothenburg & Bathurst,

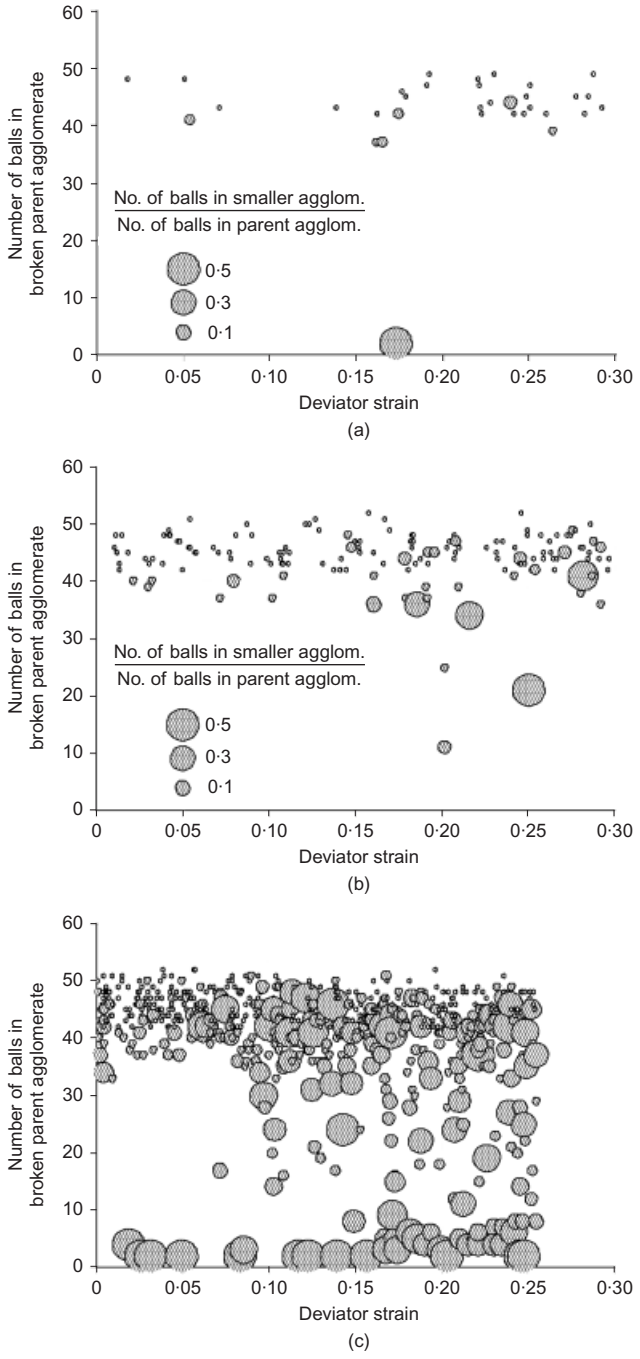

Fig. 10. Degree of fragmentation during triaxial compression: (a) 5 MPa; (b) 10 MPa; (c) 20 MPa

1992), the evolution of the internal variables of crushable grains has not been examined. It is therefore valuable to analyse and compare the variables for aggregates of breakable and unbreakable agglomerates. It should, however, be recalled that the agglomerates reported here are not only crushable; they also have much more irregular surfaces than the spherical grains reported by others.

Figure 11 shows the ratio of sliding contacts during isotropic compression. A sliding contact is defined as a contact having mobilised more than 99% of its coefficient of friction ($\mu = 0{\cdot}5$). The ratio of sliding contacts is defined as

$$\text{sliding contacts ratio} = \frac{\text{number of sliding contacts}}{\text{number of contacts between agglomerates, } C} \tag{5}$$

It is important to notice that the contacts counted in this

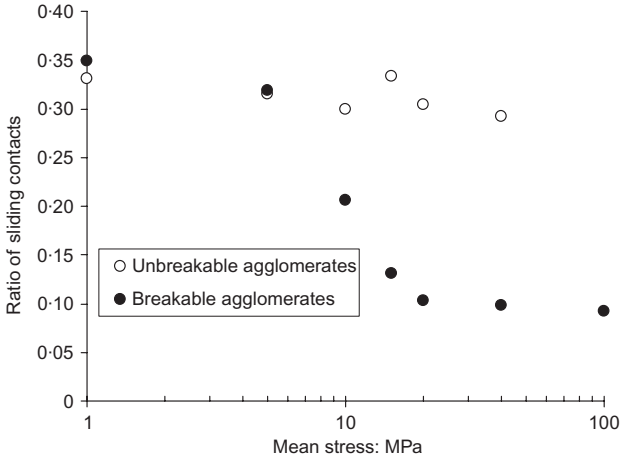

Fig. 11. Ratio of sliding contacts in isotropic compression

study are those between agglomerates, not between individual balls within agglomerates. At the outset of compression, the ratio for the breakable agglomerates had the value of 0·35, similar to that of the unbreakable agglomerates. The value in the unbreakable case remained more or less constant as mean stress increased. The value for the breakable agglomerates, however, started to drop after 5 MPa, which is where the two e–$\log p$ lines started to diverge from one another: see Fig. 4. After joining the normal compression line at 20 MPa the ratio remained constant at 0·1. Thornton (2000) showed that the sliding ratio for an assembly of spheres in a periodic cell during axisymmetric compression was virtually zero at the beginning, and remained essentially constant at 0·15 after a deviator strain of about 0·01. He did not calculate the ratio of sliding contacts during isotropic compression. Our initially higher sliding ratio might be attributed to the wide spread in contact orientations for irregular agglomerates compared with spheres. The much smaller sliding ratio in normal compression is presumed to be due to the relative significance of crushing over sliding as a means of promoting relative displacements.

The average coordination number is usually defined in terms of the number of contacts, C, and the number of agglomerates, N, as

$$Z = \frac{2C}{N} \tag{6}$$

As pointed out by Thornton (2000), there are possibly some agglomerates with zero contacts and some agglomerates that have a contact with only one neighbour. These make no mechanical contribution to the stable state. So a *mechanical* average coordination number is best calculated after Thornton (2000) as

$$Z_{\text{m}} = \frac{2C - N_1}{N - N_0 - N_1} \tag{7}$$

where N_1 and N_0 are the number of agglomerates with one and zero contacts respectively. Both coordination numbers are shown in Fig. 12. The mechanical coordination number was always larger than the conventional number by about 2. The value of the mechanical average coordination number at 1 MPa was about 6, which was the same as the value for a dense assembly of spheres compressed isotropically at 100 kPa, reported by Thornton (2000). Each coordination number shows a similar trend of increase with mean stress up to 40 MPa in isotropic compression, such that stress increasing by a factor of 10 causes the mechanical coordination number to increase to a value of 12 or higher, whether or not the agglomerates were breakable. For the case of shearing at constant mean stress, the evolution of the mech-

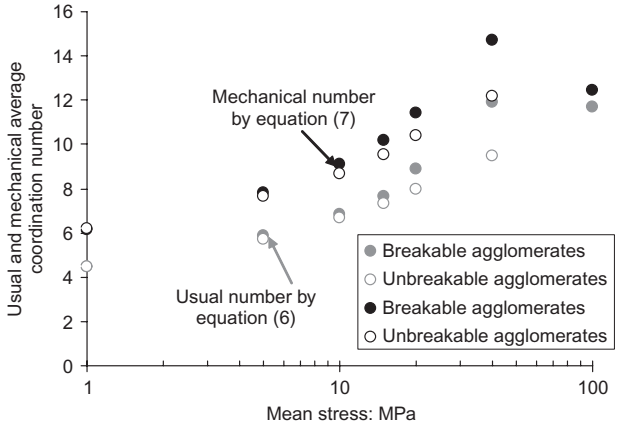

Fig. 12. Conventional and mechanical average coordination numbers in isotropic compression

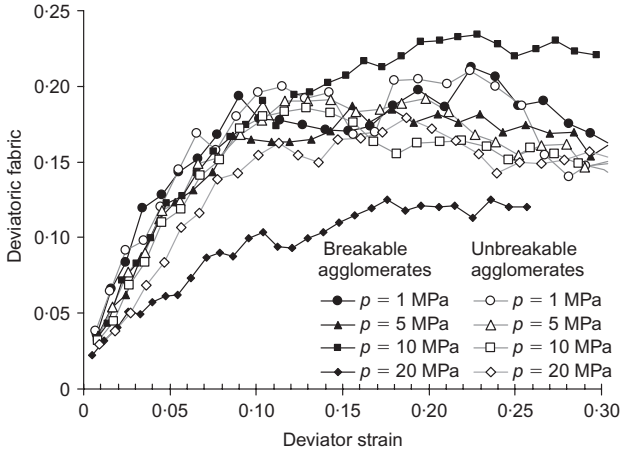

Fig. 14. Deviator fabric in triaxial compression

anical average coordination number is presented in Fig. 13. There is only a slight increase in each case.

Ng (2004a, 2004b) indicated that the coordination number for an assembly of ellipsoid grains remained in the range 4·5 to 6·0 as mean pressures increased from 2 MPa to 1000 MPa, and that the coordination number during shear tests then decreased to a final value of 4·4 to 4·6, irrespective of grain shape or initial void ratio. It might be inferred that the larger elastic deformations of the irregular porous agglomerates used in the present study were chiefly responsible for the observed increase in coordination number with mean stress, and its further gentle increase during shearing. If larger linear spring stiffnesses had been selected for ball contacts inside an agglomerate, and Herzian contact mechanics had been used for external contacts between agglomerates, then their overall elastic deformability would have been much reduced, and the coordination number would not have increased so significantly beyond 10 MPa.

Figure 14 shows the evolution of induced structural anisotropy during the triaxial compression phase of the simulations. The structural anisotropy was expressed using the definition of fabric tensor proposed by Satake (1982),

$$\phi_{ij} = \frac{1}{2C}\sum_{V} n_i n_j \tag{8}$$

where n_i and n_j denote the ith and jth components of the contact normals in the specified volume V, and C is the number of contacts for the agglomerates. The deviator fabric is then defined as the difference between the major and minor principal components of the structural anisotropy tensor, $\phi_1 = \frac{1}{2C}\sum_V n_1 n_1$ and $\phi_3 = \frac{1}{2C}\sum_V n_3 n_3$ respectively:

$$\phi_q = \phi_1 - \phi_3 \tag{9}$$

The general development of structural anisotropy with deviator strain correlates reasonably well to that presented by Thornton (2000). In addition, although the induced structural anisotropy increased with deviator strain, it decreased as the stress level increased. The figure also shows that the anisotropy of the breakable agglomerate assembly depends strongly on mean stress, being markedly smaller for states of high breakage on the normal compression line, in contrast to the unbreakable case.

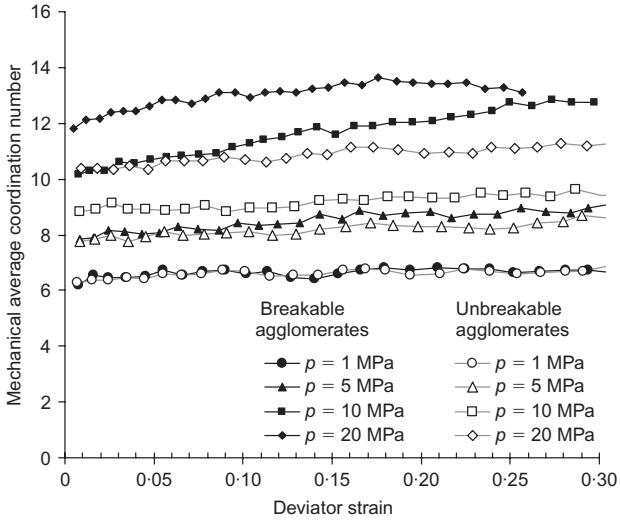

Fig. 13. Mechanical average coordination numbers in triaxial compression

WORK AND ENERGY IN AN ASSEMBLY OF AGGLOMERATES

Following the Cambridge definition of stress and strain components in a triaxial test (Roscoe *et al.*, 1963), the increment of work done per unit volume on an assembly of grains is written

$$\delta W = p\delta\varepsilon_v + q\delta\varepsilon_q \tag{10}$$

If the strain increments can be separated as elastic and plastic components, equation (3) can be written

$$\delta W = \delta U + \delta P = \left(p\delta\varepsilon_v^e + q\delta\varepsilon_q^e\right) + \left(p\delta\varepsilon_v^p + q\delta\varepsilon_q^p\right) \tag{11}$$

where the superscripts e and p denote elastic and plastic components respectively. Many experimental studies have been undertaken to comprehend the plastic work component δP. In these studies, much effort (e.g. Muhunthan & Olcott, 2002) was devoted to the precise measurement of stress and strain, and to the definition of an elastic modulus to evaluate the elastic component δU, the first bracket on the right-hand side of equation (11).

The total internal energy δS of the assembly, as demanded by Collins & Muhunthan (2003), is simply calculated as the instantaneous sum of the energies stored in the elastic spring contacts. Since the total boundary work done per unit volume δW is also calculable, the dissipation of energy δD at any stage can be deduced. It is convenient to normalise this by the current mean effective stress p, which is held constant during the compression tests reported earlier. The development of non-dimensional dissipation energy $\delta D/p$ with total deviator strain is given in Fig. 15 for the tests shown in Figs 8 and 9. The figure also shows the normalised

energy $\delta B/p$ released as a result of bond breakage in the sample subjected to triaxial compression under $p = 20$ MPa. It is important to note that the released energy $\delta B/p$ is a small fraction within the total dissipation $\delta D/p$, amounting only to about 15% of the difference in dissipation between the breakable and unbreakable agglomerate assemblies. The instantaneous release of energy caused by bond breakage is important not in itself, but in that it opens up new degrees of freedom that permit much more energy δD to be dissipated during consequent rearrangements. This agrees with the experimental considerations of McDowell *et al.* (2002).

In the Original Cam-Clay (OCC) model (Schofield & Wroth, 1968) a simple frictional dissipation function was adopted as

$$q\delta\varepsilon_{\mathrm{q}}^{\mathrm{p}} + p\delta\varepsilon_{\mathrm{v}}^{\mathrm{p}} = Mp\delta\varepsilon_{\mathrm{q}}^{\mathrm{p}} \tag{15}$$

McDowell & Bolton (1998) proposed an extended energy equation, which included a term for the increments of energy embodied in newly created surface δA_{S},

$$q\delta\varepsilon_{\mathrm{q}}^{\mathrm{p}} + p\delta\varepsilon_{\mathrm{v}}^{\mathrm{p}} = Mp\delta\varepsilon_{\mathrm{q}}^{\mathrm{p}} + \frac{\Gamma\delta A_{\mathrm{S}}}{V_{\mathrm{s}}(1+e)} \tag{16}$$

where Γ is the surface energy, and δA_{S} is the increment of surface area for a volume of solids V_{s}. The creation of surface area is directly equivalent to bond breakage in the current work, so the second term on the right-hand side of equation (15) would be equivalent to the energy δB released when bonds break. Although such a term should logically be included in the plastic work, as pointed out by McDowell *et al.* (2002), Fig. 15 has confirmed that the extra frictional dissipation δD consequent on breakage is much more important. The average gradients in Fig. 15 show that whereas $M \approx 1{\cdot}1$ is a reasonable fit for the simulations of unbreakable agglomerates, the simulations of breakable agglomerates require larger values. For the crushable assembly the coefficient M in equation (15) varies from about 1·3 in the 5 MPa test to about 1·7 in the 20 MPa test. The strong variation due to bond breakage of parameter M demonstrates that equation (15) is rather ineffective in capturing crushing effects. Cheng *et al.* (2004) showed in their figure 10(b) that the Modified Cam-Clay dissipation function in equation (12) closely satisfies the plastic work of compacting breakable agglomerates identical to those in the current simulations.

$$q\delta\varepsilon_{\mathrm{q}}^{\mathrm{p}} + p\delta\varepsilon_{\mathrm{v}}^{\mathrm{p}} = p\sqrt{\left(\delta\varepsilon_{\mathrm{v}}^{\mathrm{p}}\right)^2 + \left(M\delta\varepsilon_{\mathrm{q}}^{\mathrm{p}}\right)^2} \tag{12}$$

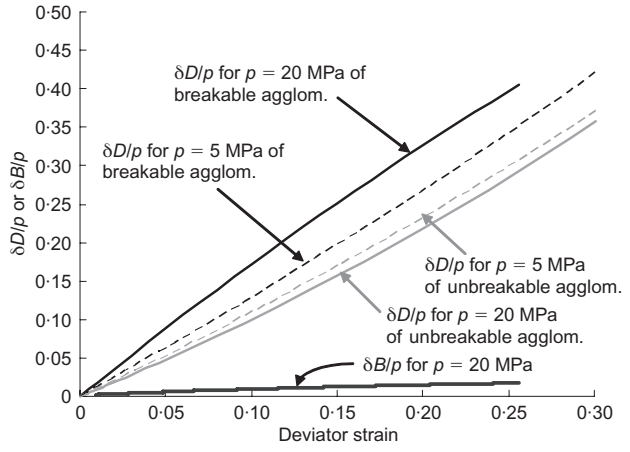

Fig. 15. Plastic work and deviator strain

CONCLUSIONS

This paper discusses the possible micro-mechanical origins of soil behaviour, based on the results of DEM simulations for irregular agglomerates of bonded balls. The discussion is based on a comparison between the results for assemblies of breakable and unbreakable numerical agglomerates. The following micro-mechanical processes were examined: energy, fragmentation process, sliding contacts ratio, coordination number, and deviatoric fabric. The conclusions are as follows.

(*a*) In the single grain-crushing simulations, an analysis was made of the modes of bond breakage and the energy balance. The bond-breaking mode was indicated by either the shear or tensile forces reaching their limit. The shear-breaking mode predominated prior to peak force, whereas the tensile mode dominated the subsequent fast fracture. The energy balance immediately before fast fracture was characterised by 75% of the boundary work ΔW being stored as elastic energy in spring contacts ΔS, with only $0{\cdot}03\Delta W$ having been released as ΔB at the instant of bond breakage. Immediately after fast fracture all stored energy had disappeared, with $0{\cdot}10\Delta W$ attributed to ΔB, while the remaining $\Delta F \approx 0{\cdot}90\Delta W$ dissipated by rearrangements consequent on bond breakage. Breakage is important not in itself but for the new movements it permits.

(*b*) The evolution of fragmentation and the mode of bond breakage was examined for an assembly of agglomerates. Before the 'yield point' in isotropic compression, the ratio of fragmentation was always small, corresponding in real grains with damage to asperities or by microcracking. An assembly of more perfect agglomerates yielded more suddenly, and exhibited unstable volume loss reminiscent of the phenomenon of 'destructuration'. After the 'yield point', when 'normal compression' on the e–$\log p$ plot gave a gradient $\lambda = 0{\cdot}4$, the fragmentation ratio of smaller agglomerates was generally high, indicating splitting, whereas larger agglomerates continued to show asperity damage with small fragmentations. In the splitting events, the tensile bond-breaking mode predominated as in single agglomerate crushing. In triaxial compression, asperity damage led to reduced dilatancy on the 'dry' side of critical states, while grain splitting of the smaller fragments contributed to volume contraction during shearing on the 'wet' side. Realistic grain size distributions were obtained.

(*c*) The sliding contacts ratio of the irregularly shaped agglomerates prior to breakage was about 0·33, compared with previously published values of about 0·15 for spherical grains. This high value is attributed to the wide spread in contact orientations: it was maintained at all stress levels for unbreakable agglomerates. As breakage began for breakable agglomerates, the sliding contacts ratio fell sharply by a factor of 3, and then remained constant during 'normal compression'. Breakage reduces the need for contact sliding when deformations are imposed.

(*d*) As mean stress in the simulations increased from 1 MPa to 100 MPa, the average coordination number doubled. A similar increase was found for the alternative definition of mechanical coordination number, logging the average numbers of contacts of agglomerates with at least two contacts. These coordination numbers increased, but very slightly, during triaxial shearing. Breakage gave a slightly greater tendency to increase coordination number, but by far the most significant effect was the mean stress, determining the elastic deformability of the agglomer-

ates irrespective of breakage. These irregular 'grains' could come into contact on many facets following slight deformations at contacts. More work is needed on the modelling of elastic grain deformation using DEM agglomerates, in the light of these large coordination numbers.

(*e*) The fabric deviator increased with deviator strain in triaxial test simulations, as expected, but this increase reduced with stress level, and even more so when breakage was permitted. Less anisotropy is induced if grains distort or break.

(*f*) The true dissipation, defined by subtracting the stored energy in elastic springs from the work input at the boundaries of an element, was found to be usefully normalised by the mean effective stress. The normalised dissipation for breakable agglomerates was significantly larger than that for unbreakable agglomerates, but the fraction of this difference that was directly attributable to the deletion of bonds was quite small (less than 10%), reflecting the energies observed in single-particle crushing. So from a micro-mechanical point of view the main effect of bond breakage was the sudden creation of new degrees of freedom, which caused more energy to be dissipated by friction and damping. Dissipation by the Modified Cam Clay model is better able to encompass grain breakage than the Original Cam Clay model.

NOTATION

B	energy lost due to bond breakage
b	bond strength
e	voids ratio
F	energy lost due to rearrangement of balls
k	contact stiffness
M	critical state stress ratio
P	irrecoverable (plastic) work
p	mean effective stress
δp	change in mean efective stress
q	deviator stress, $\sigma'_1 - \sigma'_3$
δq	change in deviator stress
S	elastic strain energy stored at points of contact
W	work input at test boundaries
U	recoverable (elastic) work
$\delta\varepsilon_q$	increment of deviator strain ($= \frac{2}{3}(d\varepsilon_1 + d\varepsilon_3)$)
$\delta\varepsilon_q^e$	increment of elastic deviator strain
$\delta\varepsilon_q^p$	increment of plastic deviator strain
$\delta\varepsilon_v$	increment of volumetric strain
$\delta\varepsilon_v^e$	increment of elastic volumetric strain
$\delta\varepsilon_v^p$	increment of plastic volumetric strain

REFERENCES

Bolton, M. D. (1986). The strength and dilatancy of sands. *Géotechnique* **36**, No. 1, 65–78.

Cheng, Y. P. (2004). *Micro-mechanical investigation of soil plasticity.* PhD thesis, University of Cambridge.

Cheng, Y. P., Nakata, Y. & Bolton, M. D. (2003). Distinct element simulation of crushable soil. *Géotechnique* **53**, No. 7, 633–641.

Cheng, Y. P., Bolton, M. D. & Nakata, Y. (2004). Crushing and plastic deformation of soils simulated using DEM. *Géotechnique* **54**, No. 2, 131–141.

Cheng, Y. P., Bolton, M. D. & Nakata, Y. (2005). Grain crushing and critical states observed in DEM simulations, *Powders and Grains 2005, Proc. 5th International Conference on Micromechanics of Granular Media, Stuttgart*, 1393–1397.

Collins, I. F. (2005). The concept of stored plastic work or frozen elastic energy in soil mechanics. *Géotechnique* **55**, No. 5, 373–382.

Collins, I. F. & Muhunthan, B. (2003). On the relationship between stress–dilatancy, anisotropy, and plastic dissipation for granular materials. *Géotechnique* **53**, No. 7, 611–618.

Cundall, P. A. & Strack, O. D. L. (1979). A discrete numerical model for granular assemblies. *Géotechnique* **29**, No. 1, 47–65.

Hettler, A. & Vardoulakis, I. (1984). Behaviour of dry sand tested in a large triaxial apparatus. *Géotechnique* **34**, No. 2, 183–198.

Leroueil, S. & Vaughan, P. R. (1990). The general and congruent effects of structure in natural soils and weak rocks. *Géotechnique* **40**, No. 3, 467–488.

Leung, C. F., Lee, F. H. & Yet, N. S. (1996). The role of particle breakage in pile creep in sand. *Can. Geotech. J.* **33**, No. 6, 888–898.

McDowell, G. R. (2002) On the yielding and plastic compression of sand. *Soils Found.* **42**, No. 1, 139–145.

McDowell, G. R. & Bolton, M. D. (1998). On the micro-mechanics of crushable aggregates. *Géotechnique* **48**, No. 5, 667–679.

McDowell, G. R. & Harireche, O. (2002a). Discrete element modelling of soil particle fracture. *Géotechnique* **52**, No. 2, 131–135.

McDowell, G. R. & Harireche, O. (2002b). Discrete element modelling of yielding and normal compression of sand. *Géotechnique* **52**, No. 4, 299–304.

McDowell, G. R., Nakata, Y. & Hyodo, M. (2002). On the plastic hardening of sand. *Géotechnique*, **52**, No. 5, 349–358.

Muhunthan, B. & Olcott, D. (2002). Elastic energy and shear work. *Géotechnique* **52**, No. 7, 541–544.

Nakata, Y., Hyodo, M., Hyde, A. F. L., Kato, Y. & Murata, H. (2001a). Microscopic particle crushing of sand subjected to high pressure one-dimensional compression. *Soils Found.* **41**, No. 1, 69–82.

Nakata, Y., Kato,Y., Hyodo, M., Hyde, A. F. L. & Murata, H. (2001b). One-dimensional compression behaviour of uniformly graded sand related to single particle crushing strength. *Soils Found.* **41**, No. 2, 39–51.

Ng, T.-T. (2004a). Triaxial simulations using DEM with hydrostatic boundaries. *J. Engng Mech. ASCE* **130**, No. 10, 1188–1194.

Ng, T.-T. (2004b). Behaviors of ellipsoids of two sizes. *J. Geotech. Geoenviron. Engng Mech. ASCE* **130**, No. 10, 1077–1083.

Ohta, H., Yoshikoshi, H., Mori, Y., Yonetani, S., Itho, M. & Ishiguro, T. (2001). Behaviour of a rockfill dam during construction. *Proc. 15th Int. Conf. Soil Mech. Geotech. Engng, Istanbul* **2**, 1227–1231.

Randolph, M. F., Dolwin, J. & Beck, R. (1994). Design of driven piles in sand. *Géotechnique* **44**, No. 3, 427–448.

Robertson, D. (2000). *Computer simulations of crushable aggregates*. PhD dissertation, University of Cambridge.

Roscoe, K. H., Schofield, A. N. & Thurairagah, A. (1963). Yielding of clays in states wetter than critical. *Géotechnique* **13**, No. 2, 211–240.

Rothenburg, L. & Bathurst, R. J. (1992). Micro-mechanical features of granular assemblies with planar elliptical particles. *Géotechnique* **42**, No. 1, 79–95.

Rowe, P. W. (1971). Theoretical meaning and observed values of deformation parameters for soil. In *Stress–strain behaviour of soils*, *Proceedings of the Roscoe Memorial Symposium* (ed. R. H. G. Parry), pp. 143–194. Henley-on-Thames: Foulis.

Satake, M. (1982). Fabric tensor in granular materials. In *Deformation and failure of granular materials* (eds P. A. Vermeer and H. J. Luger), pp. 63–68. Rotterdam: Balkema.

Schofield, A. N. & Wroth, C. P. (1968). *Critical state soil mechanics*. New York: McGraw-Hill.

Thornton, C. (2000). Numerical simulations of deviatoric shear deformation of granular media. *Géotechnique* **50**, No. 1, 43–53.

Thornton, C., Yin, K. K. & Adams, M. J. (1996). Numerical simulation of the impact fracture and fragmentation of agglomerates. *J. Phys. D: Appl. Phys.* **29**, 424–435.

Yasufuku, N. & Hyde, A. F. L. (1995). Pile end-bearing capacity in crushable sands. *Géotechnique* **45**, No. 4, 663–676.